Glucose-Induced Nuclear Shuttling of ChREBP Is Mediated by Sorcin and Ca²⁺ Ions in Pancreatic β-Cells

Nafeesa A. Noordeen, Gargi Meur, Guy A. Rutter, and Isabelle Leclerc

Carbohydrate-responsive element-binding protein (ChREBP) is a regulator of pancreatic β-cell gene expression and an important mediator of glucotoxicity. Glucose increases the activity and nuclear localization of ChREBP by still ill-defined mechanisms. Here we reveal, using both MIN6 and primary mouse β-cells, a unique mechanism behind ChREBP nuclear translocation. At low glucose concentrations, ChREBP interacts with sorcin, a penta EF hand Ca²⁺ binding protein, and is sequestered in the cytosol. Sorcin overexpression inhibits ChREBP nuclear accumulation at high glucose and reduced the activity of L-type pyruvate kinase (L-PK) and TxNIP promoters, two well-characterized ChREBP target genes. Sorcin inactivation by RNA interference increases ChREBP nuclear localization and in vivo binding to the L-PK promoter at low glucose concentrations. Ca²⁺ influx was essential for this process since Ca²⁺ chelation with EGTA, or pharmacological inhibition with diazoxide and nifedipine, blocked the effects of glucose. Conversely, mobilization of intracellular Ca²⁺ with ATP caused the nuclear accumulation of ChREBP. Finally, sorcin silencing inhibited ATP-induced increases in intracellular Ca²⁺ and glucose-stimulated insulin secretion. We therefore conclude that sorcin retains ChREBP in the cytosol at low glucose concentrations and may act as a Ca²⁺ sensor for glucose-induced nuclear translocation and the activation of ChREBP-dependent genes. *Diabetes* **61**:574–585, 2012

Carbohydrate-responsive element-binding protein (ChREBP) is a member of the basic helix-loop-helix family of transcription factors and transactivates glucose-responsive genes by binding to DNA as a heterodimer with Max-like protein ×1 at a well-defined carbohydrate-responsive element (1,2). ChREBP is responsible for converting excess carbohydrate to fatty acids for long-term storage (1). Thus, ChREBP-null mice display diminished rates of hepatic glycolysis and lipogenesis resulting in high liver glycogen content, low plasma free fatty acid levels, and reduced adipose tissue mass (3). Loss of ChREBP in *ob/ob* mice protects against obesity and hyperphagia (3,4). In the pancreatic β-cell, ChREBP overexpression (5) or silencing (6) results in the inhibition and stimulation, respectively, of glucose-stimulated insulin secretion (GSIS). These actions of ChREBP seem likely to be mediated through alterations in the deleterious effects of high glucose concentrations on β-cell function and survival,

termed glucotoxicity. The latter process may involve the induction by ChREBP of lipogenic genes such as fatty acid synthase and L-type pyruvate kinase (L-PK) (6,7), as well as the proapoptotic gene thioredoxin interacting protein *Txnip* (8,9), and suppression of critical β-cell genes such as aryl hydrocarbon receptor nuclear translocator/hypoxia inducible factor-1β (ARNT/HIF-1β) (5), Pdx-1, MafA, glucokinase, and insulin (10).

Translocation of ChREBP from the cytosol to the nucleus in response to elevated glucose concentrations has been documented in both liver (11) and clonal pancreatic β-cells (6,12,13) and is likely to be a key regulatory step in the activation of downstream genes. Although previous work in the pancreatic β-cell line INS1(832/13) has identified a glucose-sensing module in the NH₂-terminal region (12,13), the exact mechanism(s) through which glucose prompts this subcellular relocalization are still unknown (14).

Sorcin (soluble resistance-related calcium binding protein) is a 22 kDa protein, highly conserved among mammals and highly expressed in primary mouse islets (top 10th percentile of all messages as assessed by microarray and RNAseq data, G. Rutter, unpublished observations) that belongs to the penta-EF-hand family (15,16). In common with other members of this family, sorcin undergoes Ca²⁺-dependent conformational changes and translocation from cytosol to membranes where it binds to target proteins (17,18). In cardiac and skeletal muscle, sorcin interacts with the ryanodine receptor (RyR) (19) and with the pore-forming α₁-subunit of voltage-dependent L-type Ca²⁺ channels (20). Sorcin has been shown to inhibit RyR activity (21), and therefore to play a role in terminating the Ca²⁺-induced Ca²⁺ release process (22,23), which would otherwise feed forward and deplete intracellular Ca²⁺ stores (24). It is noteworthy that sorcin phosphorylation by cAMP-dependent protein kinase (PKA) significantly decreases its ability to modulate RyR activity (21).

Here we show that, in the excitable pancreatic β-cell, ChREBP is sequestered in the cytosol through sorcin binding at low glucose concentrations. Upon stimulation with glucose and activation of Ca²⁺ influx, or application of ATP as an intracellular Ca²⁺-mobilizing agent, ChREBP rapidly translocates to the nucleus. In sorcin-silenced cells, ChREBP is constitutively present in the nucleus, and both glucose and Ca²⁺ are ineffective in stimulating further ChREBP nuclear shuttling.

RESEARCH DESIGN AND METHODS

Plasmids and viruses. Plasmids c-*myc*–ChREBP(WT) and c-*myc*–Pdx-1 have been described elsewhere (5,25). Plasmid c-*myc*–ChREBP(1–242) was generated by digesting c-*myc*–ChREBP(WT) by *Xba*I and self-ligation. Plasmids pGBKT7-ChREBP and pChREBP-enhanced green fluorescent protein (EGFP) were generated by subcloning full-length ChREBP cDNA in frame with the Gal4 DNA binding domain and EGFP, respectively, at the *Sal*1 sites of pGBKT7 and pEGFP-C2 (Clontech). Plasmid sorcin-HA was derived from the yeast vector pGADT7 (see below) using the following primers: forward, 5′-CGA AGC TTA TGG CGT ATC CGG GAC-3′ and reverse, 5′-ATG TGC GGC CGC GGC ATA GTC TGG

GAC GTC ATA TGG ATA GAC GGT CAT GAC ACA CTG GAT G-3, HA tag underlined, and subcloned at *Sal*I and *Not*I sites of pcDNA3.1$^+$ (Invitrogen). Plasmids −183LPK.luci and −148LPK.luci have been described in Ref. 26. Plasmid −1081TXNIP.luci was obtained from Addgene and described in Ref. 27. Adenovirus sorcin-HA, also expressing GFP from a single bicistronic mRNA under the cytomegalovirus (CMV) promoter, was generated by three-piece ligation of sorcin-HA and IRES-EGFP in pShuttle-CMV (28) using *Bgl*II, *Xho*I, and *Xba*I restriction sites. Adenovirus production was then performed as in Ref. 28. Sorcin (sc-41017-v) and control (sc-108080) short hairpin RNA (shRNA) mouse lentiviruses were purchased from Santa Cruz. All constructs were verified by DNA sequencing.

Cell culture and transfection. Human embryonic kidney 293, MIN6, and INS1 (832/13) cells were cultured as in Ref. 5 unless specified otherwise. Cells were transfected using Lipofectamine 2000 for plasmids and RNAiMAX for small interfering RNA (siRNA) (final concentration 2.5 to 5 nM) in Opti-Mem (Invitrogen).

MIN6 β-cells cDNA library generation. MIN6 cDNA library was generated according to Matchmaker Library Construction and Screening Kit (Clontech) using Oligo d(T) primers, 2.0 µg total RNA, yeast strain AH109, and pGADT7-Rec AD. The transformants were selected on SD/-leu plates before yeast mating.

Two-hybrid screen. Yeast two-hybrid was performed according to Matchmaker Gal4 Two-Hybrid System 3 (Clontech). In brief, yeast mating was performed using yeast strain AH109 containing the MIN6 cDNA library, and yeast strain Y187 was pretransformed with pGBKT7-ChREBP. Screens were conducted at high (-adenine/-histidine/-leucine/-tryptophan) stringency with 5 mmol/L 3-AT to prevent background growth. The library cDNAs contained in pGADT7 were identified by sequencing.

Coimmunoprecipitation and Western (immuno-) blotting. Cells were transfected with plasmid vectors encoding c-*myc*–ChREBP(WT), c-*myc*–ChREBP(1–242), c-*myc*–Pdx-1 and sorcin-HA, or sorcin-HA alone for 48 h before coimmunoprecipitation with mouse anti–c-*myc* and Western blotting as described in Ref. 29 using either mouse anti–c-*myc*, mouse anti-HA, or mouse anti-sorcin antibodies.

Chemical crosslinking analysis. MIN6 β-cells were cultured for 16 h in 3 mmol/L glucose followed by 3 h in 3 or 30 mmol/L glucose. The cells were washed twice with PBS and incubated with 1 mmol/L disuccinimidyl suberate (Pierce), at room temperature, for 30 min. The crosslinker reaction was quenched by incubating with 20 mmol/L Tris (pH 7.4) for 15 min at room temperature, followed by washing twice with ice-cold PBS. The cells were lysed in Nonidet-40 lysis buffer before immunoprecipitation with anti-sorcin antibody and Western blotting as above.

Chromatin immunoprecipitation assay. MIN6 β-cells were transfected with scrambled or specific sorcin siRNA for 48 h. Chromatin immunoprecipitation was performed using anti-ChREBP antibody and mouse L-PK promoter primers as described (5,6).

Nuclear-cytosolic protein extraction. MIN6 β-cells, nontransfected or transfected with sorcin-HA for 48 h, were cultured for 16 h in 3 mmol/L glucose followed by 6 h in 3 or 30 mmol/L glucose. The cells were scraped in ice-cold PBS, followed by centrifuging at 500*g* for 2 min. The cell pellets were lysed, and nuclear proteins were separated from the cytosolic fraction using the NucBuster Protein Extraction Kit (Novagen) before Western blotting.

Luciferase assays. MIN6 β-cells seeded in 24-well plates were transfected with 1.5 µg of either −183LPK.luci, −148LPK.luci, or −1081TXNIP.luci reporter plasmids, 0.5 µg of either GFP or sorcin cDNA, and 1.5 ng of renilla luciferase to correct for transfection efficiency, using Lipofectamine 2000 (Invitrogen) and OPTI-MEM (5 mmol/L glucose) for 24 h followed by 25 mmol/L glucose Dulbecco's modified Eagle's medium for 24 h before cell lysis and luciferase assay using Dual-Luciferase Reporter Assay System (Promega).

Immunostaining and confocal microscopy. MIN6 β-cells were fixed in 4% (volume for volume) paraformaldehyde, permeabilized with 0.3% Triton X-100, and stained with rabbit anti–c-*myc* antibody (1:250; Santa Cruz), and mouse anti-HA antibody (1:1000; 12CA5, Roche), followed by Alexa 488 conjugated goat anti-rabbit IgG and Alexa 568 conjugated donkey anti-mouse IgG (1:1,000; Invitrogen). Cells were imaged using a Zeiss Axiovert 200M microscope fitted with a PlanApo ×63 oil immersion objective. Confocality was achieved using a Nipkow spinning disc under the control of Volocity 4.0 (Improvision) software.

Measurement of free cystolic intracellular Ca^{2+}. MIN6 β-cells were loaded with fura-2 A.M. (2 µmol/L in DMSO) in Krebs-Ringer bicarbonate HEPES (KRBH) buffer (125 mmol/L NaCl, 3.5 mmol/L KCl, 1.5 mmol/L CaCl$_2$, 0.5 mmol/L MgSO$_4$, 0.5 mmol/L NaH$_2$PO$_4$, 25 mmol/L NaHCO$_3$, and 10 mmol/L HEPES), supplemented with 3 mmol/L glucose for 60 min at 37°C. Cells were perifused in KRBH and imaged at 37°C using an Olympus IX-70 with an Imago charge-coupled device camera (Till Photonics, Grafelfing, Germany) controlled by TILLvisION software (Till Photonics). Cells were illuminated alternately for 5 ms at 340 and 380 nm, and the emission was filtered at 510 nm. After background and auto-fluorescence were subtracted (by quenching with 10 mmol/L MnCl$_2$ and 1 µmol/L ionomycin), free cystolic intracellular Ca^{2+} ([Ca^{2+}]$_{cyt}$) was calculated using a look-up table created from standard Ca^{2+} solutions (Molecular Probes).

Live-cell confocal imaging of ChREBP-EGFP. MIN6 β-cells were transfected either with ChREBP-EGFP plasmid alone or with sorcin siRNA for 48 h. Cells were then incubated overnight with 3 mmol/L glucose Dulbecco's modified Eagle's medium, and subsequently the coverslips were rinsed with 3 mmol/L glucose KRBH buffer and mounted on a hot stage with continuous perifusion with warm KRBH. Cells were imaged using a Zeiss Axiovert 200M microscope (Carl Zeiss, Jena, Germany) fitted with a PlanApo 63× oil-immersion objective and a 1.5 Optivar attached to a Nokigawa spinning disc confocal head. Hoechst (Invitrogen) staining of nuclei was visualized through DAPI filter. GFP-expressing samples were illuminated using steady-state 488 nm laser line, and emission was collected through ET535/30 emission filter (Chroma) for every 5 s. Images were captured using a Hamamatsu EM charge-coupled device digital camera, model C9100-13, controlled by Volocity 4.0 software. Deconvoluted images were analyzed by obtaining the gray values for every time point in the region of interest drawn around nucleus and the cytosol, which was then corrected for background and normalized, and ratios of nuclear to cytosolic distribution were generated.

Preparation and imaging of dissociated mouse islets. Mouse islets were isolated (5) and partially dissociated by incubation in Hank's based cell dissociation buffer (Invitrogen) for 10 min by gentle pipetting. To assess the effects of intracellular Ca^{2+}, primary cell clusters were transduced with c-*myc*–ChREBP-expressing adenoviral particles (also expressing GFP) (5) at a multiplicity of infection of ~50 for 6 h, followed by 48 h culture in fresh medium. Dissociated islets were then incubated overnight in 3 mmol/L glucose and thereafter in 3 or 17 mmol/L glucose in KRBH buffer containing either 1.5 mmol/L CaCl$_2$ or 10 mmol/L EGTA for 30 min and fixed in 4% paraformaldehyde for 10 min. After permeabilization with 0.1% Triton × 100, immunostaining was carried out using the following antibodies: monoclonal anti–c-*myc* antibody (1:200; Roche), polyclonal anti-swine insulin (1:200; DakoCytomation, Ely, UK), and Alexa 564 or 633-coupled secondary antibodies (1:1,000; Molecular Probes), and coverslips were mounted in VECTASHIELD (Vector Laboratories) hardset medium with DAPI. Imaging was performed using a Leica SP2 upright confocal microscope with an HCX PL APO 63× 1.32 numerical aperture oil immersion objective and the following laser lines: Argon ion (488 nm), HeNe (633 nm), 561 nm diode, and ultraviolet (350 nm) controlled by Leica LAS AF Lite software. Acquired images were analyzed using Volocity software (Improvision). To assess the effect of sorcin over-expression or silencing on endogenous ChREBP nuclear localization, dissociated islets were transduced with either sorcin (also expressing GFP) or GFP adenoviral particles as above or with shRNA sorcin or control lentiviral particles (Santa Cruz) according to the manufacturer's instructions in 11 mmol/L glucose RPMI 1640 for 48 h followed by 1 h in 3 mmol/L glucose RPMI 1640 and 6 h in 17 mmol/L glucose RPMI 1640. Cells were then fixed and immunostained using rabbit anti-ChREBP (1:100; Thermo Scientific) and mouse anti-sorcin (1:50; Invitrogen) and secondary goat–anti-rabbit Alexa 568, and goat–anti-mouse Alexa 633 (both at 1:1,000; Invitrogen).

Insulin secretion and assay. MIN6 β-cells were transfected with sorcin-specific or scrambled siRNAs for 48 h before insulin secretion assay (5).

Statistical analysis. Data are given as mean ± SEM of at least three individual experiments. Comparisons between means were performed using two-tailed Student *t* test for unpaired data, with Bonferroni correction and ANOVA.

RESULTS

ChREBP and sorcin are molecular binding partners under physiological conditions. We first detected sorcin as a ChREBP interactor in a yeast two-hybrid screen using full length ChREBP as bait in a pancreatic β-cell MIN6 library (not shown). We confirmed the interaction in mammalian cells by coimmunoprecipitation experiments of overexpressed c-*myc*–tagged ChREBP and HA-tagged sorcin in human embryonic kidney 293 cells (Supplementary Fig. 1) and INS-1(832/13) β-cells (Fig. 1*A*, first lane from left). This interaction was further delimited to the first 242 amino acids of ChREBP (Fig. 1*A*, second lane), a region known as the low-glucose inhibitory domain (12). Establishing the specificity of the ChREBP-sorcin interaction, coimmunoprecipitation experiments did not reveal any interaction between sorcin-HA and c-*myc*–Pdx-1 (Fig. 1*A*, fourth lane), a transcription factor that also translocates to the nucleus in response to high glucose in this cell type (25).
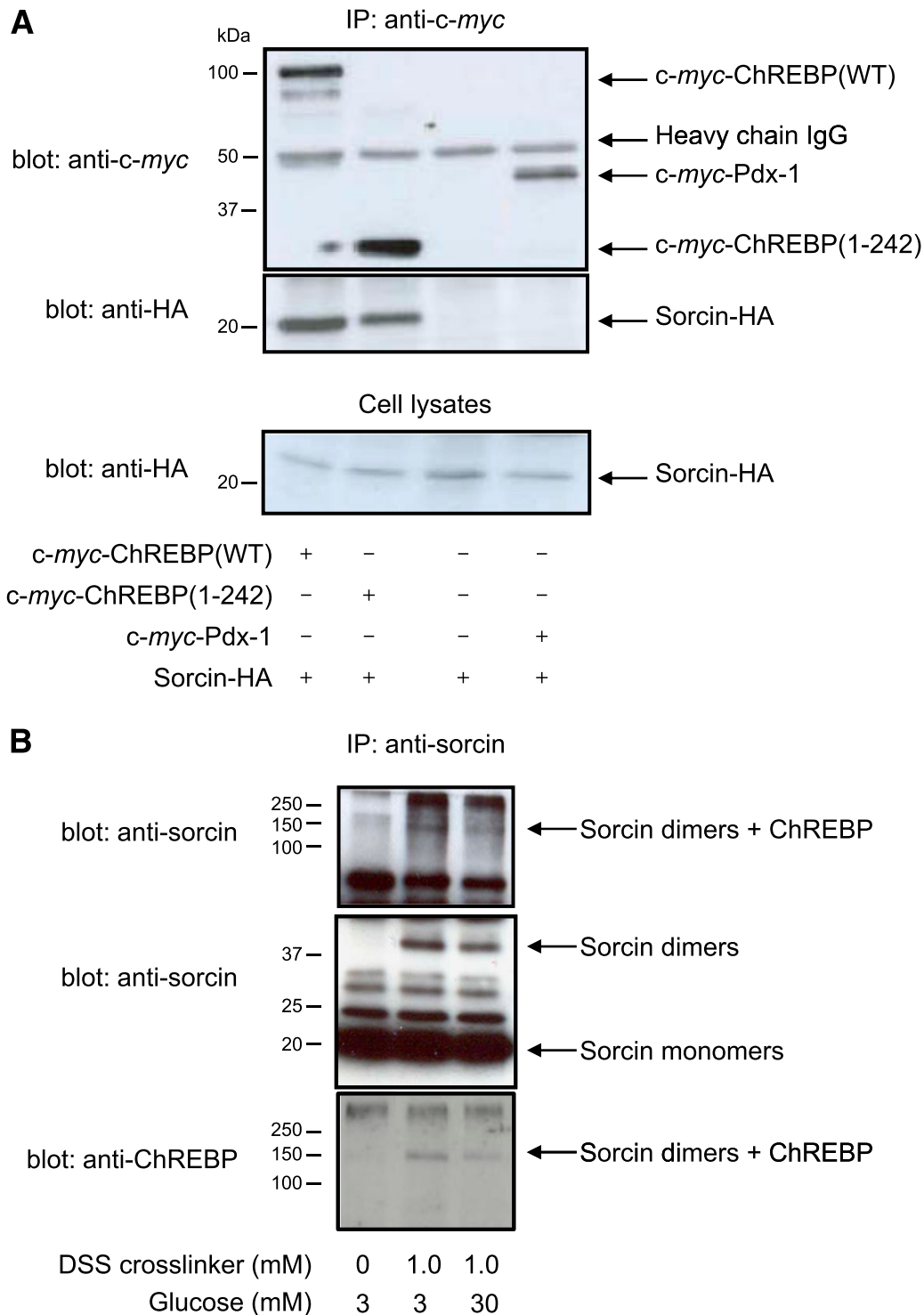
FIG. 1. ChREBP and sorcin are molecular interactors in pancreatic β-cells. *A*: Overexpressed ChREBP and sorcin coimmunoprecipitate. INS1 (832/13) β-cells were cotransfected with c-*myc*–ChREBP(WT), c-*myc*–ChREBP(1–242) or c-*myc*–Pdx-1, and sorcin-HA or sorcin-HA alone as indicated underneath the figure, before immunoprecipitation with anti–c-*myc* antibody, and Western blotting using anti–c-*myc* (*top*) or anti-HA (*middle*) antibodies. Ten percent of cell lysates were probed with anti-HA antibody as input control (*bottom*). *B*: Chemical crosslinking of endogenous ChREBP and sorcin. MIN6 β-cells were cultured in 3 mmol/L glucose for 16 h, followed by 3 or 30 mmol/L glucose for 3 h before crosslinking with disuccinimidyl suberate (DSS) and cell lysis as described in RESEARCH DESIGN AND METHODS. Cell lysates were immunoprecipitated with anti-sorcin antibody. After SDS PAGE and blotting onto nitrocellulose, the blots were probed with anti-sorcin (*top* and *middle*) or anti-ChREBP antibodies (*bottom*). These are representative blots of 3 independent experiments. IP, immunoprecipitation. (A high-quality color representation of this figure is available in the online issue.)

We next explored the interaction between endogenous ChREBP and sorcin in MIN6 cells. Such interaction was only detectable after crosslinking experiments, as shown in Fig. 1B. Indeed, crosslinking and immunoprecipitation with anti-sorcin antibody revealed a high molecular complex of ~140 kDa using both anti-sorcin (Fig. 1B, top panel, second and third lanes) and anti-ChREBP (Fig. 1B, bottom panel, second and third lanes) antibodies. We believe this
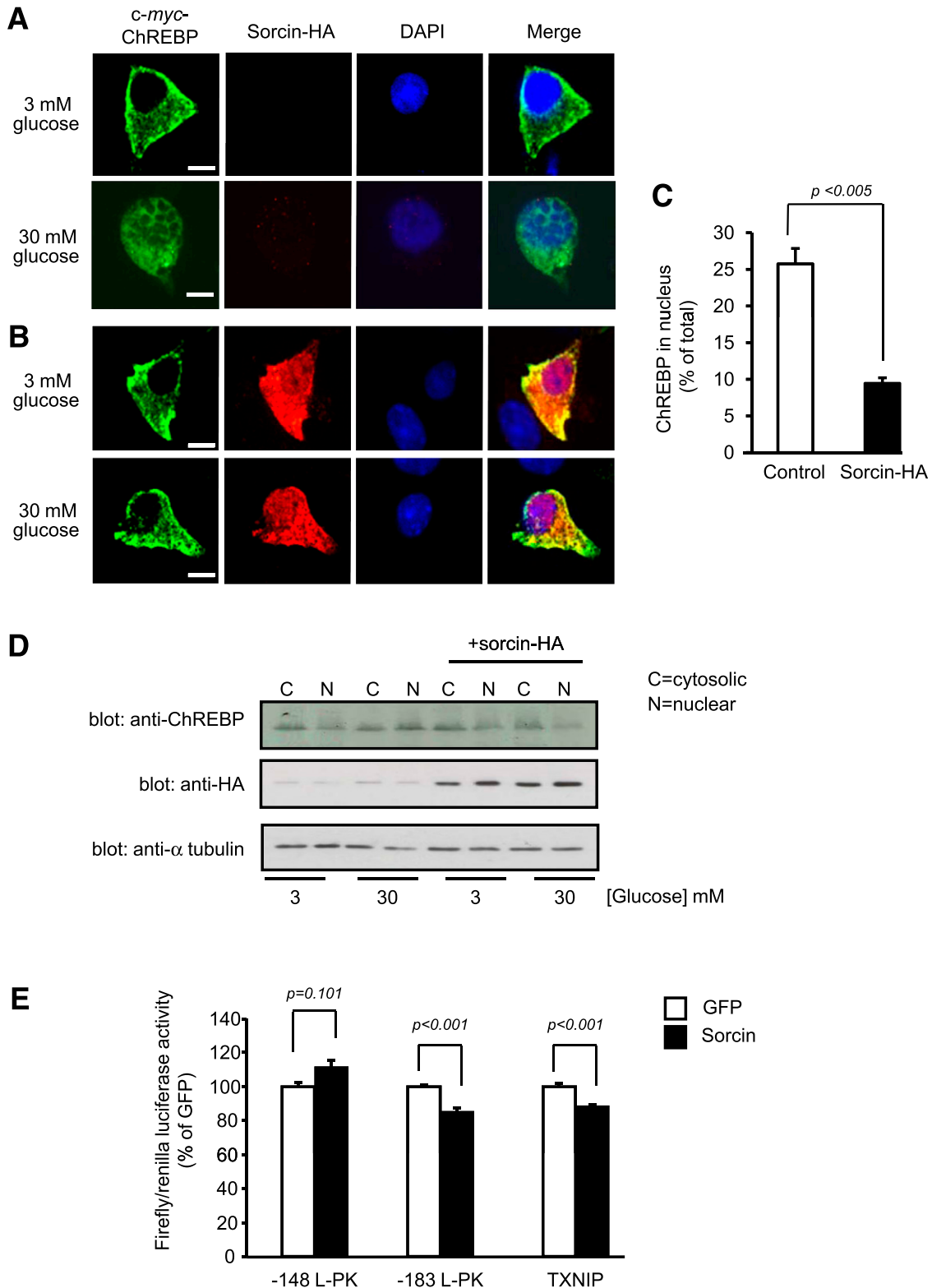
FIG. 2. Sorcin colocalizes with ChREBP in MIN6 β-cells and controls its subcellular localization. *A* and *B*: MIN6 β-cells were transfected with c-*myc*–ChREBP alone (*A*) or in combination with sorcin-HA (*B*) and cultured in either 3 or 30 mmol/L glucose for 6 h as indicated. Immunocytochemistry and confocal imaging were performed as described in RESEARCH DESIGN AND METHODS. Scale bars = 5 μm. *C*: Quantification of c-*myc*–ChREBP in the nucleus, for the 30 mmol/L glucose experiments presented in *A* and *B*. The intensities of c-*myc* staining were measured using Volocity 4.0 software, for both nuclear and cytoplasmic regions of interest, in each individual cell, and background intensities were subtracted. Nuclear ChREBP intensity is expressed as percentage of cytoplasmic intensity ($n \geq 3$ experiments, with 30 cells per condition). *D*: MIN6 β-cells were transfected with sorcin-HA in 25 mmol/L Dulbecco's modified Eagle's medium for 48 h before culturing in 3 mmol/L glucose for 16 h, followed by 3 or 30 mmol/L glucose for 6 h. The nuclear and cytosolic fractions were extracted, and Western blots were performed as described in RESEARCH DESIGN AND METHODS. The blots were probed with anti-ChREBP (*top*), anti-HA (*middle*), or anti–α-tubulin antibodies (*bottom*). The experiment was repeated twice with similar results. *E*: MIN6 β-cells were cotransfected with either −148L-PK luci, −183L-PK luci, or −1081TXNIP luci together with GFP or sorcin as indicated before cell lysis and luciferase assays as described in RESEARCH DESIGN AND METHODS (n = 3 to 8). GFP, green fluorescent protein. (A high-quality digital representation of this figure is available in the online issue.)
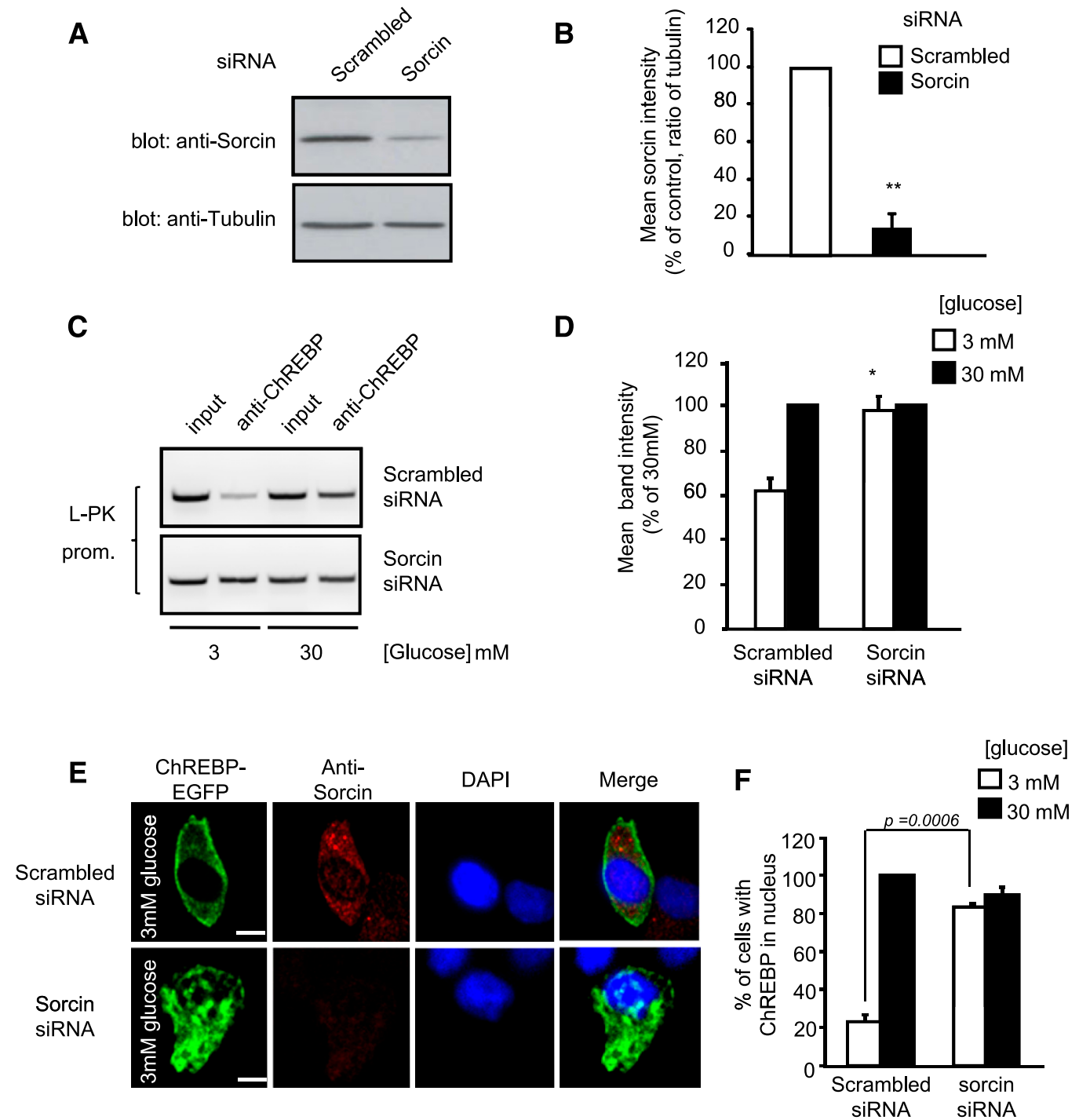
FIG. 3. Sorcin is necessary for ChREBP cytosolic localization. *A* and *C*: MIN6 β-cells were transfected with sorcin-specific or scrambled siRNAs (2.5 nmol/L for 48 h) before cell lysis, SDS PAGE, and Western blot using anti-sorcin and anti–α-tubulin antibodies (*A*) or crosslinking and chromatin immunoprecipitation assay using primers amplifying the proximal L-PK promoter (*C*) as described in RESEARCH DESIGN AND METHODS. *B*: Quantification of three separate Western blots presented in *A*, using ImageJ. The intensity values were normalized to α-tubulin and expressed as percentage of scrambled siRNA. *D*: Quantification of 3 separate chromatin immunoprecipitation (ChIP) experiments presented in *C*, using ImageJ, and expressed as percentage of 30 mmol/L. *E*: MIN6 β-cells were transfected with EGFP-ChREBP in combination with either scrambled or sorcin siRNAs and imaged as in Fig. 2. Scale bars = 5 μm. *F*: Number of cells that displayed a nuclear-localized ChREBP counted from experiments in *E* (*n* = 30–40 cells/condition). prom., promoter. **P < 0.005, *P < 0.05 for the effects of sorcin siRNA. (A high-quality digital representation of this figure is available in the online issue.)

complex to represent sorcin dimers and ChREBP, since sorcin dimers were also detected after addition of the crosslinker (Fig. 1*B*, middle panel, second and third lanes). **Sorcin acts as a cytosolic anchor for ChREBP.** It has been shown previously that ChREBP constantly shuttles between the cytosol and the nucleus (13). The cytosolic

retention domain has been mapped to the NH₂-terminal region of ChREBP, since NH₂-terminal deletion mutants lacking the first 252 amino acids are predominantly nuclear (12,30,31).

Because sorcin interacts with ChREBP specifically through this domain (see Fig. 1*A*), we next investigated
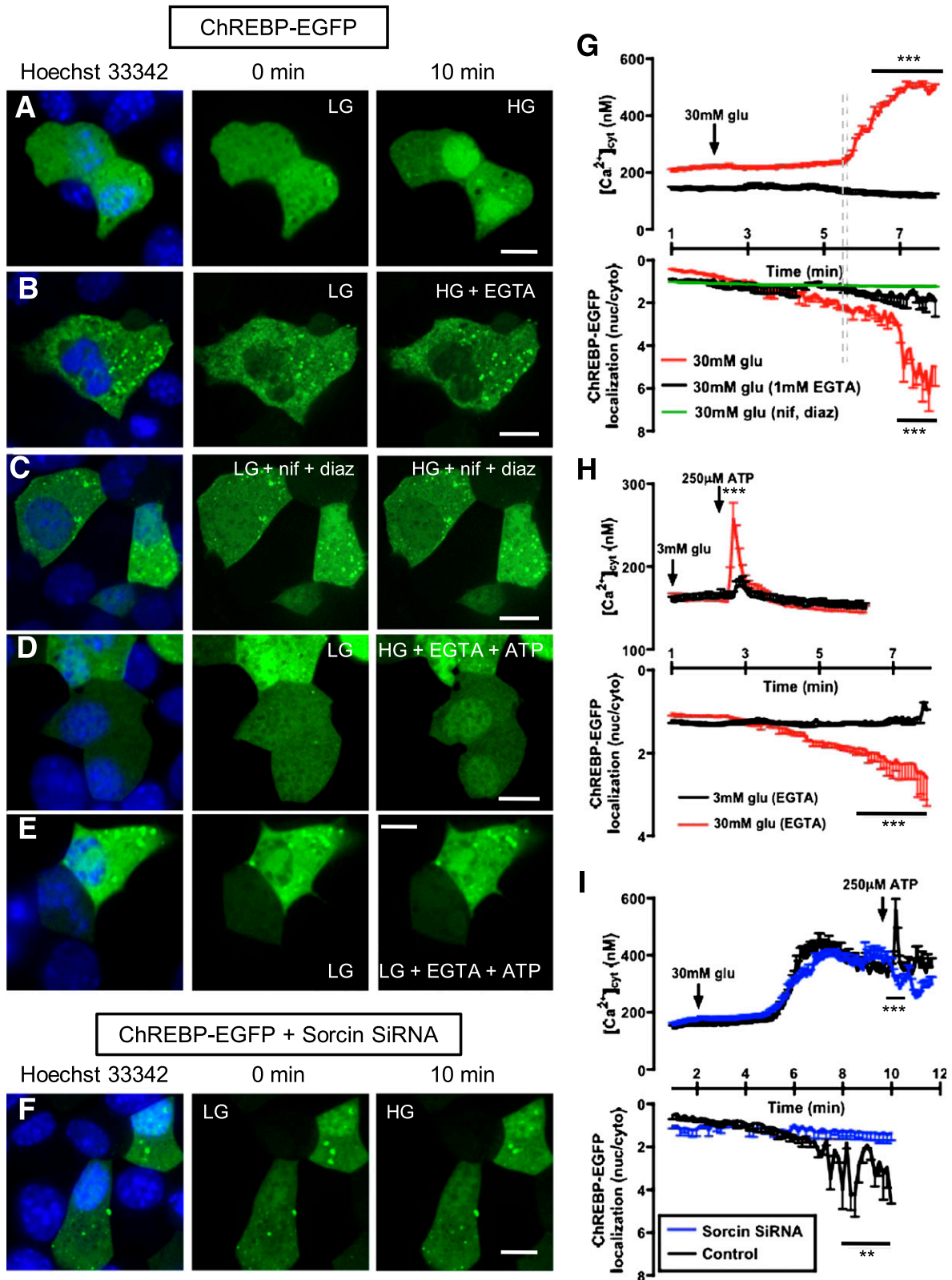
FIG. 4. ChREBP-EGFP nuclear translocation evoked by [Ca²⁺]$_{cyt}$ requires sorcin for coupling of the events. *A-F*: Live-cell images of ChREBP-EGFP in MIN6 β-cells (typical of *n* ≥7–10 cells) expressed either alone or in combination with sorcin siRNA (*F*; *n* >10). All cells starved (3 mmol/L glucose) overnight and were imaged while perifusing with indicated buffers in warm KRBH. In *C*, cells were preincubated (10 min) with nifedipine (nif; 10 μmol/L) and diazoxide (diaz; 250 μmol/L) before imaging. Unless specified as Ca²⁺-free (containing EGTA), all buffers contained 1.5 mmol/L Ca²⁺. Scale bar = 10 μm. *G-I* (upper panels): [Ca²⁺]$_{cyt}$ signals evoked by glucose (*G, I*) and ATP (*H, I*). Traces show the responses from ≥30 cells (≥55 for sorcin-silenced cells), taken from at least 3 independent experiments (means ± SEM). *G-I* (bottom panels): Real-time quantification of ChREBP-EGFP (gray values) in nuclear and cytosolic compartments. Traces (scale reversed to time-match events in the upper panel) show average from ≥10 cells (*I*; ≥30) during various treatments, from 3 independent experiments (means ± SEM). nuc, nucleus; cyto, cytosol; glu, glucose. **P < 0.005, ***P < 0.0005 for the effects of treatments. (A high-quality digital representation of this figure is available in the online issue.)

whether sorcin may play a role in controlling the subcellular localization of ChREBP. With the use of spinning disc confocal microscopy, c-*myc*–ChREBP immunoreactivity was examined in MIN6 β-cells transfected with either c-*myc*–ChREBP alone or cotransfected with c-*myc*–ChREBP and sorcin-HA and incubated at low or high glucose concentrations. As expected from the coimmunoprecipitation experiments presented above, ChREBP and sorcin immunoreactivities extensively colocalized, especially at low glucose concentrations (Fig. 2B). Strikingly, however, sorcin overexpression greatly diminished the abundance of ChREBP staining in the nucleus from 25.7 ± 2.1% in the control cells to 9.4 ± 0.8% in the sorcin overexpressed cells ($P < 0.005$, Fig. 2C), suggesting that sorcin may serve as a cytosolic anchor for ChREBP. This was also observed in cell fractionation experiments where sorcin overexpression reduced ChREBP immunoreactivity in the nuclear compartment of cells incubated in elevated glucose concentration (Fig. 2D). Moreover, sorcin overexpression significantly reduced the activity of the −183L-PK and TXNIP promoters, two well-characterized ChREBP target genes (6,9) in luciferase reporter assays, whereas a truncated L-PK promoter (−148L-PK), lacking the ChREBP binding site, was unaffected by sorcin (Fig. 2E).

We next examined the effects of sorcin silencing on ChREBP binding to the L-PK promoter by chromatin immunoprecipitation (ChIP) and subcellular localization in response to glucose. Using siRNA, we achieved a reduction of ~86% of sorcin immunoreactivity (Fig. 3A and B). As reported previously (6), glucose (30 vs. 3 mmol/L) stimulation increased ChREBP binding on the proximal L-PK promoter (Fig. 3C, top panel). In contrast, in sorcin-silenced cells, ChREBP binding to the L-PK promoter was constitutive, irrespective of glucose concentrations (Fig. 3C, bottom panel, and Fig. 3D for quantification). Accordingly, inactivation of sorcin by RNAi led to an increase in the number of cells displaying nuclear ChREBP-EGFP

fluorescence at resting (3 mmol/L) glucose concentration (83.3 ± 2.9% vs. 23.3 ± 4.0%, $P < 0.001$; Fig. 3E and F).

These results designate sorcin as a physiological regulator of ChREBP activity in response to glucose in MIN6 cells.

Elevated glucose concentrations, Ca^{2+} influx, and sorcin are all necessary for ChREBP nuclear translocation. Because sorcin undergoes conformational changes after Ca^{2+} binding (18), we next tested whether Ca^{2+} influx in response to glucose or other agents would drive ChREBP into the nucleus. Imaged dynamically in living MIN6 β-cells, elevated glucose concentrations caused a rapid translocation of ChREBP-EGFP from the cytosol to the nucleus (Fig. 4A and G and Supplementary Movie 1). Parallel single-cell measurements of $[Ca^{2+}]_{cyt}$ revealed that nuclear accumulation of ChREBP closely followed (~1 min) a glucose-evoked Ca^{2+} signal ($\Delta[Ca^{2+}]_{cyt} = 312 \pm 14$ nmol/L; Fig. 3G). Chelation of extracellular Ca^{2+} with 1 mmol/L EGTA (Fig. 4B and G and Supplementary Movie 2) abolished glucose-induced Ca^{2+} entry and thereby Ca^{2+}-induced nuclear translocation of ChREBP, which was also suppressed by 10 μmol/L nifedipine, an L-type Ca^{2+} channel blocker, and by 250 μmol/L diazoxide, an activator of ATP-sensitive K$^+$ channels (Fig. 4C and G and Supplementary Movie 3) that prevent membrane depolarization and subsequent Ca^{2+} entry. Furthermore, a transient Ca^{2+} peak ($\Delta[Ca^{2+}]_{cyt} = 108 \pm 11$ nmol/L) elicited by 250 μmol/L extracellular ATP, an activator of G protein–coupled P2 purinergic receptors (32), led to robust cytosol-nuclear shuttling of ChREBP in the absence of extracellular Ca^{2+} (Fig. 4D and H and Supplementary Movie 4), suggesting that mobilization of intracellular Ca^{2+} stores was sufficient for translocation. Apparently, nuclear translocation of ChREBP also depended upon the presence of elevated concentrations (30 mmol/L) of glucose (Fig. 4E and Supplementary Movie 5), but this largely reflected the increased Ca^{2+} release ($\Delta[Ca^{2+}]_{cyt} = 31 \pm 7$ nmol/L at low vs. 108 ± 11 nmol/L at high glucose) in these conditions (Fig. 4H).
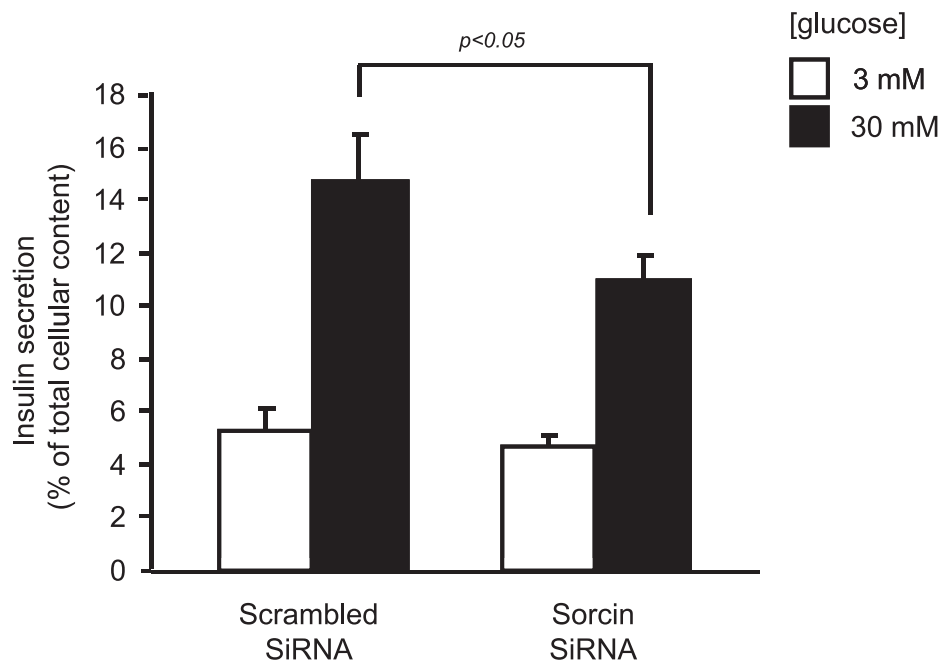

FIG. 5. Sorcin silencing decreases glucose-stimulated insulin secretion in MIN6 β-cells. MIN6 β-cells were transfected with sorcin-specific or scrambled siRNAs before insulin secretion assay as described in RESEARCH DESIGN AND METHODS. Data are means ± SEM from 3 separate experiments.

We next examined the effects of sorcin silencing on ChREBP nuclear translocation in response to elevated glucose concentrations and Ca^{2+} signals. Although glucose-induced $\Delta[Ca^{2+}]_{cyt}$ were not significantly different (330 ± 20 vs. 280 ± 22 nmol/L for control and sorcin-silenced cells, $P = 0.55$), glucose stimulation failed to trigger nuclear shuttling of ChREBP in sorcin-silenced cells (Fig. 4F and Supplementary Movie 6). On the contrary, a high level of ChREBP was already detected in the nucleus, even before treatments, pointing to the role of sorcin as a ChREBP cytosolic anchor as discussed above. Silencing of sorcin also completely abolished ATP-evoked Ca^{2+} release from intracellular stores ($\Delta[Ca^{2+}]_{cyt} = 234 \pm 20$ nmol/L for control vs. -54 ± 18 nmol/L for sorcin-siRNA; Fig. 4I).

Sorcin knockdown inhibits GSIS. We next examined the impact of sorcin inhibition on GSIS. As shown in Fig. 5, sorcin silencing significantly decreased GSIS in pancreatic MIN6 β-cells.

Calcium influx is required to cause ChREBP nuclear translocation in primary mouse β-cells in response to glucose. We next examined the effects of Ca^{2+} influx and sorcin in primary β-cells. Dissociated CD1 mouse islets were transduced with c-*myc*–tagged ChREBP-expressing adenoviral particles (5) for 48 h and incubated overnight in 3 mmol/L glucose and thereafter in 3 or 17 mmol/L glucose KRBH containing either 1.5 mmol/L $CaCl_2$ or 10 mmol/L EGTA for 30 min before immunostaining and imaging as described in RESEARCH DESIGN AND METHODS. The identity of the β-cells was established by simultaneous immunostaining with insulin antibody. As shown in Fig. 6, inhibiting Ca^{2+} influx also abolished ChREBP nuclear localization in response to glucose.
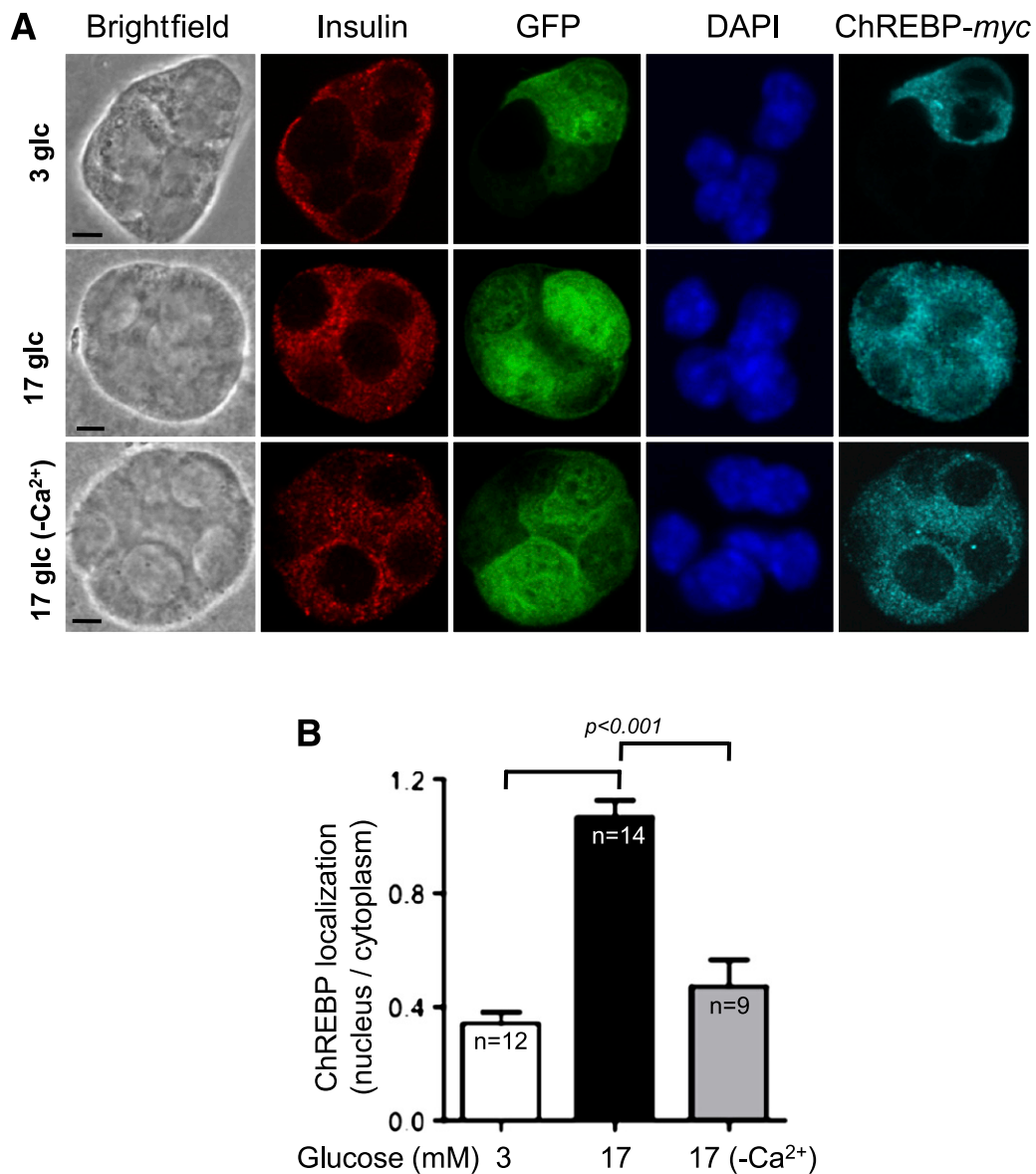

FIG. 6. Glucose- and Ca^{2+}-mediated ChREBP translocation in mouse primary β-cells. *A*: Confocal images (single z-section of 0.45 µm) of partially dissociated mouse islet β-cell clusters immunostained with insulin and c-*myc* antibodies as described in RESEARCH DESIGN AND METHODS. Cells were starved overnight in 3 mmol/L glucose and subsequently incubated in KRBH buffer (either with 1.5 mmol/L $CaCl_2$ or 10 mmol/L EGTA) containing 3 or 17 mmol/L glucose for 30 min as stated in the figure. Scale bar, 5 µm. *B*: Fluorescence emission (>700 nm) from the region of interest drawn around the nucleus and cytoplasm were calculated, and ratio was derived. Mean ± SEM from the stated number of clusters combined with single cells, from 3 separate experiments. glc, glucose. (A high-quality digital representation of this figure is available in the online issue.)

Sorcin controls ChREBP subcellular location in primary mouse β-cells. Extending the physiological relevance of the above findings, sorcin overexpression in dissociated primary mouse islets (comprising 70–80% β-cells) (33) diminished endogenous ChREBP nuclear immunoreactivity from $28.6 \pm 1.5\%$ in control cells to $16.5 \pm 1.0\%$ in sorcin overexpressing cells incubated in elevated (17 mmol/L) glucose ($P < 0.001$, Fig. 7A and B). Conversely, sorcin silencing increased endogenous ChREBP nuclear staining to $25.5 \pm 1.4\%$ compared with $13.6 \pm 1.1\%$ in control cells ($P < 0.001$, Fig. 7C and D), incubated in low (3 mmol/L) glucose.

DISCUSSION

The chief goal of the current study was to elucidate the molecular mechanisms through which elevated glucose concentrations lead to the nuclear accumulation of ChREBP in the pancreatic β-cell. We show that sorcin provides a Ca^{2+}-regulated cytosolic anchor, likely to play an important role in the regulation of this process in both clonal and primary β-cells.

In the liver, glucose-dependent ChREBP nuclear translocation is subject to a series of phosphorylation/dephosphorylation reactions. In fasting and in low glucose conditions, ChREBP is phosphorylated by PKA on S196 and T666 and by AMP-activated protein kinase on S568, which promote cytosol retention and inhibit DNA binding. By contrast, in high glucose conditions, protein phosphatase 2A activation by xylulose 5-phosphate (34) induces dephosphorylation of S196, T666, and S568; nuclear import; and DNA binding (35,36). Dephosphorylation of these residues, however, was not sufficient for ChREBP nuclear translocation in the glucose-responsive pancreatic β-cell line INS1 (832/13) (13). This is unsurprising, since, in the pancreatic β-cell, elevated glucose concentrations are rather associated with protein phosphatase 2A inhibition (37,38) and increased intracellular cAMP levels and PKA signaling (39,40), pointing to the existence of additional mechanisms, possibly including the inhibition by glucose of AMP-activated protein kinase (41).

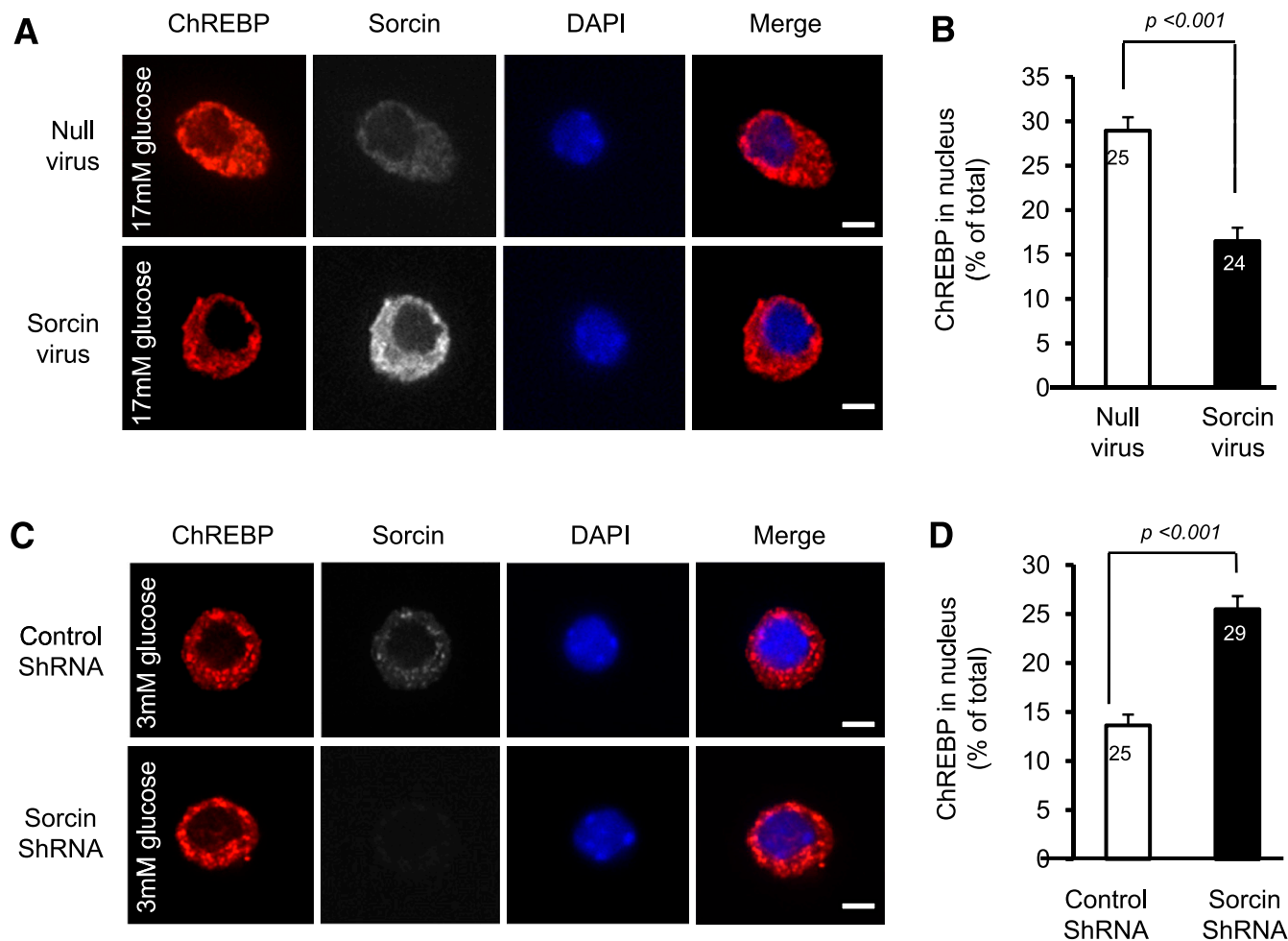Here we show that, in the excitable pancreatic β-cell, elevated glucose concentrations provoke ChREBP nuclear

FIG. 7. Sorcin controls ChREBP subcellular location in primary mouse β-cells. *A:* Dissociated mouse islets were transduced for 48 h with null or sorcin-overexpressing adenoviruses in 11 mmol/L glucose RPMI 1640, and then incubated 1 h in 3 mmol/L glucose followed by 6 h in 17 mmol/L RPMI 1640, before immunochemistry and confocal imaging as described in RESEARCH DESIGN AND METHODS. Scale bars = 5 μm. *C:* Dissociated mouse islets were transduced with control or sorcin-shRNA lentiviruses for 72 h in 11 mmol/L RPMI 1640 and then incubated for 6 h in 3 mmol/L RPMI 1640 before immunochemistry and confocal imaging as above. *B* and *C:* Quantification of endogenous ChREBP in the nucleus, for the experiments presented in *A* and *C*. The intensities of ChREBP staining were measured using Volocity 4.0 software, for both nuclear and cytoplasmic regions of interest, in each individual cell, and background intensities were subtracted. Nuclear ChREBP intensity is expressed as percentage of cytoplasmic intensity ($n = 3$ experiments, with 24 to 29 cells per condition). (A high-quality digital representation of this figure is available in the online issue.)

translocation through stimulation of Ca^{2+} influx. Thus, extracellular Ca^{2+} chelation with EGTA or pharmacological blockade of Ca^{2+} entry with diazoxide or nifedipine completely abolished glucose-induced ChREBP nuclear shuttling, both in clonal MIN6 (Fig. 4) and primary mouse β-cells (Fig. 6). Conversely, mobilization of intracellular Ca^{2+} with extracellular ATP was sufficient to cause ChREBP nuclear translocation. Together, these data point to a central role for $[Ca^{2+}]_{cyt}$ in this phenomenon. Critically, we show that overexpression or silencing of sorcin in clonal (Fig. 2–4) or primary (Fig. 7) β-cells blocks and inhibits, respectively, nuclear accumulation of ChREBP, implicating sorcin as a likely sensor of cytosolic Ca^{2+}.

Changes in $[Ca^{2+}]_{cyt}$ have been reported previously to be detected and decoded as nuclear events via mechanisms involving cytosol-nuclear translocation of nuclear factor activator of transcription and nuclear factor-κB cells (NF-κB) (42). The signaling module reported here may represent a similar system, which allows highly localized changes in cytosolic Ca^{2+}, perhaps close to the ER or even a specific Ca^{2+} release channel, to be decoded as a transcriptional response. We thus propose a model (Fig. 8) in which sorcin, a penta-EF-hand protein that undergoes Ca^{2+}-dependent conformational changes (15–18), binds to and sequesters ChREBP in the cytosol at low glucose, through an interaction with the NH_2-terminal domain of ChREBP. After glucose stimulation and Ca^{2+}-induced Ca^{2+} release, sorcin liberates ChREBP, which is then free to translocate to the nucleus. The regulation of ARNT/HIF-1β gene in pancreatic β-cells supports this model of ChREBP activation. Indeed, we have recently shown that ChREBP is a repressor of ARNT/HIF-1β promoter in pancreatic β-cells (5), whereas another group (43) has shown that blocking Ca^{2+} flux from intracellular Ca^{2+} channels induces the expression of ARNT/HIF-1β in this cell type.

Other interesting findings of this study are the apparent depletion of intracellular Ca^{2+} stores (Fig. 4I) and the inhibition of GSIS (Fig. 5) after sorcin silencing in MIN6 cells. The absence of sorcin may lead to a depletion of intracellular Ca^{2+} stores by allowing random activation of RyR (21). Another possibility would be a change in gene expression, possibly the expression of the G protein–coupled P2 purinergic receptors, hence diminishing the response to extracellular ATP. However, any such changes were apparently efficiently countered by modifications to Ca^{2+} pumping since neither resting nor glucose-stimulated increases in cytosolic Ca^{2+} were perturbed by the knockdown of sorcin (Fig. 4I). It follows that the interaction of sorcin with voltage-dependent (L-type) Ca^{2+} channels (20) in the β-cell may be of limited importance in the control of Ca^{2+} influx. The latter observation argues against substantial changes in β-cell glucose metabolism or in cellular viability after sorcin silencing in the short period (48 h) of our study. However, a chronic sorcin inhibition is likely to induce changes in gene expression through a constitutive ChREBP signaling pathway, including downregulation of ARNT/HIF-1β (5) and upregulation of TxNIP (9). Although the latter is often associated with oxidative stress and cell death by mechanisms involving mitochondrial Ca^{2+} accumulation (44), we would note that the possible depletion of ER Ca^{2+} stores (see above), required in several cell types for efficient accumulation of mitochondrial Ca^{2+} (45), may reduce
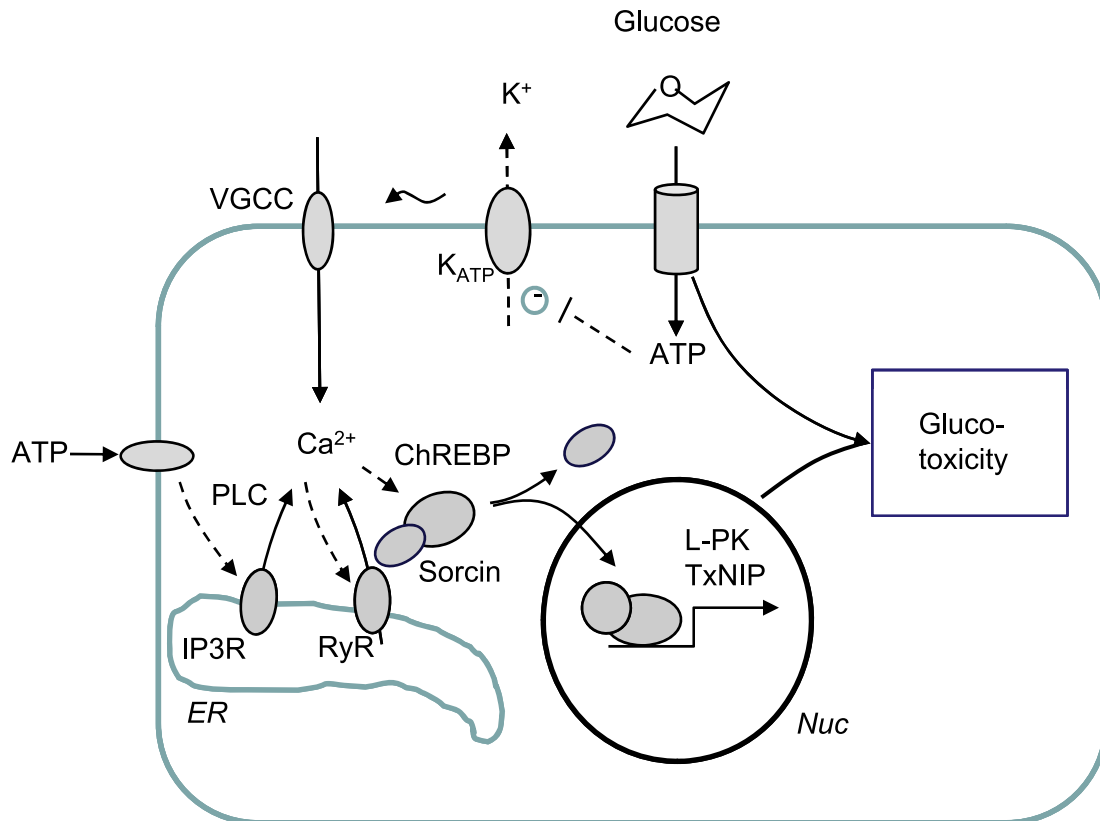

FIG. 8. Proposed model of ChREBP activation via sorcin and Ca^{2+} ions. High glucose and subsequent Ca^{2+}-induced Ca^{2+} release (CICR) cause ChREBP and sorcin dissociation in the cytosol. Activated ChREBP then translocates into the nucleus where it activates transcription. IP3R, inositol 1,4,5-trisphosphate receptors; ER, endoplasmic reticulum; RyR, ryanodine receptors; PLC, phospholipase C; VGCC, voltage-gated calcium channels; Nuc, nucleus. (A high-quality color representation of this figure is available in the online issue.)

the magnitude of any proapoptotic effects of TxNIP induction. Further detailed studies will be required in the future to discriminate between these possibilities.

An event distal to increase in $[Ca^{2+}]_{cyt}$ is therefore likely to be involved in the inhibition of GSIS. This may, for example, include the less efficient mobilization or fusion of secretory granules with the plasma membrane in sorcin-silenced cells (46).

An exciting corollary of the work presented here is the development of novel therapeutic approaches involving sorcin activators or sorcin overexpression in the treatment of failing β-cells in type 2 diabetes, which may complement the positive action of such agents in the heart (47,48).

REFERENCES

1. Uyeda K, Repa JJ. Carbohydrate response element binding protein, ChREBP, a transcription factor coupling hepatic glucose utilization and lipid synthesis. Cell Metab 2006;4:107–110
2. Stoeckman AK, Ma L, Towle HC. Mlx is the functional heteromeric partner of the carbohydrate response element-binding protein in glucose regulation of lipogenic enzyme genes. J Biol Chem 2004;279:15662–15669
3. Iizuka K, Bruick RK, Liang G, Horton JD, Uyeda K. Deficiency of carbohydrate response element-binding protein (ChREBP) reduces lipogenesis as well as glycolysis. Proc Natl Acad Sci USA 2004;101:7281–7286
4. Dentin R, Benhamed F, Hainault I, et al. Liver-specific inhibition of ChREBP improves hepatic steatosis and insulin resistance in ob/ob mice. Diabetes 2006;55:2159–2170
5. Noordeen NA, Khera TK, Sun G, et al. Carbohydrate-responsive element-binding protein (ChREBP) is a negative regulator of ARNT/HIF-1β gene expression in pancreatic islet β-cells. Diabetes 2010;59:153–160
6. da Silva Xavier G, Rutter GA, Diraison F, Andreolas C, Leclerc I. ChREBP binding to fatty acid synthase and L-type pyruvate kinase genes is stimulated by glucose in pancreatic beta-cells. J Lipid Res 2006;47:2482–2491
7. Wang H, Wollheim CB. ChREBP rather than USF2 regulates glucose stimulation of endogenous L-pyruvate kinase expression in insulin-secreting cells. J Biol Chem 2002;277:32746–32752
8. Chen J, Hui ST, Couto FM, et al. Thioredoxin-interacting protein deficiency induces Akt/Bcl-xL signaling and pancreatic beta-cell mass and protects against diabetes. FASEB J 2008;22:3581–3594
9. Cha-Molstad H, Saxena G, Chen J, Shalev A. Glucose-stimulated expression of Txnip is mediated by carbohydrate response element-binding protein, p300, and histone H4 acetylation in pancreatic beta cells. J Biol Chem 2009;284:16898–16905
10. da Silva Xavier G, Sun G, Qian Q, Rutter GA, Leclerc I. ChREBP regulates Pdx-1 and other glucose-sensitive genes in pancreatic β-cells. Biochem Biophys Res Commun 2010;402:252–257
11. Ishii S, Iizuka K, Miller BC, Uyeda K. Carbohydrate response element binding protein directly promotes lipogenic enzyme gene transcription. Proc Natl Acad Sci USA 2004;101:15597–15602
12. Li MV, Chang B, Imamura M, Poungvarin N, Chan L. Glucose-dependent transcriptional regulation by an evolutionarily conserved glucose-sensing module. Diabetes 2006;55:1179–1189
13. Davies MN, O'Callaghan BL, Towle HC. Glucose activates ChREBP by increasing its rate of nuclear entry and relieving repression of its transcriptional activity. J Biol Chem 2008;283:24029–24038
14. Postic C, Dentin R, Denechaud PD, Girard J. ChREBP, a transcriptional regulator of glucose and lipid metabolism. Annu Rev Nutr 2007;27:179–192
15. Valdivia HH. Modulation of intracellular Ca^{2+} levels in the heart by sorcin and FKBP12, two accessory proteins of ryanodine receptors. Trends Pharmacol Sci 1998;19:479–482
16. Ilari A, Johnson KA, Nastopoulos V, et al. The crystal structure of the sorcin calcium binding domain provides a model of Ca^{2+}-dependent processes in the full-length protein. J Mol Biol 2002;317:447–458
17. Maki M, Kitaura Y, Satoh H, Ohkouchi S, Shibata H. Structures, functions and molecular evolution of the penta-EF-hand Ca^{2+}-binding proteins. Biochim Biophys Acta 2002;1600:51–60
18. Appelblom H, Nurmi J, Soukka T, et al. Homogeneous TR-FRET high-throughput screening assay for calcium-dependent multimerization of sorcin. J Biomol Screen 2007;12:842–848
19. Meyers MB, Pickel VM, Sheu SS, Sharma VK, Scotto KW, Fishman GI. Association of sorcin with the cardiac ryanodine receptor. J Biol Chem 1995;270:26411–26418
20. Meyers MB, Puri TS, Chien AJ, et al. Sorcin associates with the pore-forming subunit of voltage-dependent L-type Ca^{2+} channels. J Biol Chem 1998;273:18930–18935
21. Lokuta AJ, Meyers MB, Sander PR, Fishman GI, Valdivia HH. Modulation of cardiac ryanodine receptors by sorcin. J Biol Chem 1997;272:25333–25338
22. Fabiato A. Calcium-induced release of calcium from the cardiac sarcoplasmic reticulum. Am J Physiol 1983;245:C1–C14
23. Farrell EF, Antaramian A, Rueda A, Gómez AM, Valdivia HH. Sorcin inhibits calcium release and modulates excitation-contraction coupling in the heart. J Biol Chem 2003;278:34660–34666
24. Stern MD, Cheng H. Putting out the fire: what terminates calcium-induced calcium release in cardiac muscle? Cell Calcium 2004;35:591–601
25. Rafiq I, Kennedy HJ, Rutter GA. Glucose-dependent translocation of insulin promoter factor-1 (IPF-1) between the nuclear periphery and the nucleoplasm of single MIN6 beta-cells. J Biol Chem 1998;273:23241–23247
26. Kennedy HJ, Viollet B, Rafiq I, Kahn A, Rutter GA. Upstream stimulatory factor-2 (USF2) activity is required for glucose stimulation of L-pyruvate kinase promoter activity in single living islet beta-cells. J Biol Chem 1997;272:20636–20640
27. Rani S, Mehta JP, Barron N, et al. Decreasing Txnip mRNA and protein levels in pancreatic MIN6 cells reduces reactive oxygen species and restores glucose regulated insulin secretion. Cell Physiol Biochem 2010;25:667–674
28. He TC, Zhou S, da Costa LT, Yu J, Kinzler KW, Vogelstein B. A simplified system for generating recombinant adenoviruses. Proc Natl Acad Sci USA 1998;95:2509–2514
29. Noordeen NA, Carafoli F, Hohenester E, Horton MA, Leitinger B. A transmembrane leucine zipper is required for activation of the dimeric receptor tyrosine kinase DDR1. J Biol Chem 2006;281:22744–22751
30. Merla G, Howald C, Antonarakis SE, Reymond A. The subcellular localization of the ChoRE-binding protein, encoded by the Williams-Beuren syndrome critical region gene 14, is regulated by 14-3-3. Hum Mol Genet 2004;13:1505–1514
31. Sakiyama H, Wynn RM, Lee WR, et al. Regulation of nuclear import/export of carbohydrate response element-binding protein (ChREBP): interaction of an alpha-helix of ChREBP with the 14-3-3 proteins and regulation by phosphorylation. J Biol Chem 2008;283:24899–24908
32. Lee PS, Squires PE, Buchan AM, Yuen BH, Leung PC. P2-purinoreceptor evoked changes in intracellular calcium oscillations in single isolated human granulosa-lutein cells. Endocrinology 1996;137:3756–3761

33. Meur G, Qian Q, da Silva Xavier G, et al. Nucleo-cytosolic shuttling of FoxO1 directly regulates mouse Ins2 but not Ins1 gene expression in pancreatic beta cells (MIN6). J Biol Chem 2011;286:13647–13656

34. Kabashima T, Kawaguchi T, Wadzinski BE, Uyeda K. Xylulose 5-phosphate mediates glucose-induced lipogenesis by xylulose 5-phosphate-activated protein phosphatase in rat liver. Proc Natl Acad Sci USA 2003;100:5107–5112

35. Kawaguchi T, Takenoshita M, Kabashima T, Uyeda K. Glucose and cAMP regulate the L-type pyruvate kinase gene by phosphorylation/dephosphorylation of the carbohydrate response element binding protein. Proc Natl Acad Sci USA 2001;98:13710–13715

36. Kawaguchi T, Osatomi K, Yamashita H, Kabashima T, Uyeda K. Mechanism for fatty acid "sparing" effect on glucose-induced transcription: regulation of carbohydrate-responsive element-binding protein by AMP-activated protein kinase. J Biol Chem 2002;277:3829–3835

37. Palanivel R, Veluthakal R, Kowluru A. Regulation by glucose and calcium of the carboxylmethylation of the catalytic subunit of protein phosphatase 2A in insulin-secreting INS-1 cells. Am J Physiol Endocrinol Metab 2004;286:E1032–E1041

38. Parameswara VK, Sule AJ, Esser V. Have we overlooked the importance of serine/threonine protein phosphatases in pancreatic beta-cells? Role played by protein phosphatase 2A in insulin secretion. JOP 2005;6:303–315

39. Rabinovitch A, Grill V, Renold AE, Cerasi E. Insulin release and cyclic AMP accumulation in response to glucose in pancreatic islets of fed and starved rats. J Clin Invest 1976;58:1209–1216

40. Tian G, Sandler S, Gylfe E, Tengholm A. Glucose- and hormone-induced cAMP oscillations in α- and β-cells within intact pancreatic islets. Diabetes 2011;60:1535–1543

41. Leclerc I, Rutter GA. AMP-activated protein kinase: a new β-cell glucose sensor? Regulation by amino acids and calcium ions. Diabetes 2004;53 (Suppl. 3):S67–S74

42. Dolmetsch RE, Xu K, Lewis RS. Calcium oscillations increase the efficiency and specificity of gene expression. Nature 1998;392:933–936

43. Dror V, Kalynyak TB, Bychkivska Y, et al. Glucose and endoplasmic reticulum calcium channels regulate HIF-1beta via presenilin in pancreatic beta-cells. J Biol Chem 2008;283:9909–9916

44. Chen J, Fontes G, Saxena G, Poitout V, Shalev A. Lack of TXNIP protects against mitochondria-mediated apoptosis but not against fatty acid-induced ER stress-mediated β-cell death. Diabetes 2010;59:440–447

45. Rutter GA, Tsuboi T, Ravier MA. Ca^{2+} microdomains and the control of insulin secretion. Cell Calcium 2006;40:539–551

46. Rutter GA. Visualising insulin secretion. The Minkowski Lecture 2004. Diabetologia 2004;47:1861–1872

47. Suarez J, Belke DD, Gloss B, et al. In vivo adenoviral transfer of sorcin reverses cardiac contractile abnormalities of diabetic cardiomyopathy. Am J Physiol Heart Circ Physiol 2004;286:H68–H75

48. Frank KF, Bölck B, Ding Z, et al. Overexpression of sorcin enhances cardiac contractility in vivo and in vitro. J Mol Cell Cardiol 2005;38:607–615